Highly homogeneous core–sheath polyaniline nanofibers obtained by polymerisation on a wire-shaped template†

Rossella Castagna,[a] Roberto Momentè,[a] Giorgio Pariani,[b] Giuseppe Zerbi,[a] Andrea Bianco[b] and Chiara Bertarelli*[a,c]

Received 23rd May 2014,
Accepted 8th August 2014

Introduction

One-dimensional nanomaterials, in particular nanofibers and nanofibrous nonwovens, are unique nanostructures with extraordinary potential in the technological context[1] and in medical application.[2,3] Filtering,[4,5] functionalization of textiles,[6] fiber reinforcement,[7,8] catalysis,[9] drug delivery,[10] wound healing[11,12] and tissue engineering[13,14] are just some examples of new opportunities. Among the different technologies[15,16] to afford nanorods, nanowires or nanofibers, electrospinning is the only one which enables the fabrication of continuous polymer fibers with diameters down to a few nanometers.[17–19] The high surface to volume ratio of nanofibers, which improves the material sensitivity with respect to the bulk, combined with a relative large productivity, makes electrospun nanofibers very attractive for sensing.[20,21] In electrospun materials, chemical sensing[22,23] has been demonstrated when intrinsic conducting polymers (ICP), such as polyaniline (PANI), are employed.[24] The interest towards PANI comes from its versatile synthesis[25,26] and doping chemistry,[27,28] high conductivity[29,30] and excellent environmental stability.[31] Moreover, in contrast to classical metallic conductors or polymeric insulators, PANI can be reversibly switched by protonation and deprotonation between a semiconductive emeraldine base form and a conductive emeraldine salt.[32–34] Different composites with gold[35] or silver[36] nanoparticles embedded into the PANI polymer have been recently reported. Furthermore, PANI/ composite systems were proposed as active filters of hazardous elements in water, such as mercury[37,38] and chromium(VI).[39,40] Unfortunately, the process to produce PANI fibers is not straightforward. To overcome this issue, several approaches have been reported.[41] Strategies include blending PANI with a polymer which supports the fiber formation.[42–45] However, the presence of this insulating component often prevents high electrical conductivities from being achieved. Although the supporting material can be removed by a selective rinsing,[46] the fibrous morphology can be strongly affected by this post-processing. Core–sheath PANI fibers with excellent morphology and remarkable conductivity have been demonstrated by means of coaxial electrospinning[47–49] that, however, requires a careful optimization to gain control over the process.

Another interesting method to obtain core–sheath nanofibers with an outer conductive polymer consists of the

[a]*Dipartimento di Chimica Materiali e Ingegneria Chimica "G. Natta", Politecnico di Milano, piazza Leonardo da Vinci 32, 20133 Milano, Italy.*

E-mail: chiara.bertarelli@polimi.it

[b]*Istituto Nazionale di Astrofisica, Osservatorio Astronomico di Brera, via E. Bianchi 46, 23807 Merate, Italy*

[c]*Center for Nano Science and Technology @PoliMi, Istituto Italiano di Tecnologia, Via Pascoli 70/3, 20133 Milano, Italy*

† Electronic supplementary information (ESI) available: SEM and optical images, UV-vis reflectance spectra, FT-IR spectra and assignment of the main IR bands.

production of a polymer mat to act as a template and the subsequent *in situ* polymerization of monomers to form a sheath of an intrinsically conducting polymer grown onto the template.[50,51] This approach has been employed in the case of polypyrroles[52,53] and also in the case of PANI, with the polymerization of the latter being performed in solution with a two-step process, namely the diffusion of the monomer onto the fiber surface followed by the oxidative polymerization of the adsorbed monomer by addition of ammonium persulfate in an acidic medium.[21,47,50] As a matter of fact, the process leads to rough fiber surfaces and not uniform fiber mats. Moreover, PANI particle deposition often occurs not only onto the fiber template but also between fibers and randomly in the mat, which results in poor quality of the final coating.

In this paper we demonstrate the production of emeraldine salt (ES) defect-free PANI nanofibers produced through a novel and simple approach. The polymer membrane is prepared by the spontaneous segregation of *N*-phenyl-1,4-phenylenediamine (ADPA) onto the Nylon 6 fiber surface during the electrospinning and the subsequent polymerization of this template upon immersion into a solution containing an oxidant agent and an acidic species. A doping process leads to PANI fibers in the ES form. The presence of the aniline dimer only on the template surface drives the formation of a homogeneous PANI sheath on the fiber template, disabling any polymerization out of the fibers. As a result, PANI self-standing membranes with exceptionally uniform and smooth fiber morphology are attained.

Experimental method

Materials

Nylon 6 in pellets, formic acid (puriss. p.a., ~98%), iron(III) chloride anhydrous ($FeCl_3$), iron(III) hexahydrate ($FeCl_3{\cdot}6H_2O$), *N*-phenyl-*p*-phenylenediamine 98% (ADPA), ammonium persulfate (APS, 98%), acetone (≥99.5%), oxalic acid (≥99%), hydrochloric acid (37%) and *p*-toluenesulfonic acid monohydrate (*p*-TSA, ≥98.5%) were purchased from Sigma Aldrich. All reagents were used as received.

Preparation of the feed solutions

N-FeA – *Nylon 6 and $FeCl_3$ anhydrous*: Nylon 6 pellets (15 wt% with respect to formic acid) were dissolved in formic acid, and then anhydrous iron chloride (5.6 wt% with respect to formic acid) was added.

N-FeH – *Nylon 6 and $FeCl_3{\cdot}6H_2O$*: Nylon 6 pellets (15 wt% with respect to formic acid) were dissolved in formic acid, and then hexahydrate iron chloride (8.85 wt% with respect to formic acid) was added.

N-sFeH – *Nylon 6 and segregated $FeCl_3{\cdot}6H_2O$*: Nylon 6 pellets and hexahydrate iron chloride were separately dissolved in formic acid and acetone, respectively. The Nylon 6 concentration was set at 25 wt% (with respect to formic acid), while the $FeCl_3{\cdot}6H_2O$ concentration was 8.85 wt% (with respect to Nylon 6). Acetone and formic acid were taken in a 2 : 7 (v/v) ratio. Once total dissolution was reached, the two solutions were mixed and the mixture was magnetically stirred until a homogeneous phase was obtained.

N-sADPA – *Nylon 6 and segregated N-phenyl-1,4-phenylenediamine (ADPA)*: Nylon 6 pellets were dissolved in formic acid, while separately ADPA was dissolved in acetone. The Nylon 6 concentration was set at 25 wt% (with respect to formic acid), while different concentrations of ADPA were considered (48, 54, 60.5, 67, 73 wt% with respect to Nylon 6). Acetone and formic acid were taken in a 2 : 7 (v/v) ratio. Once total dissolution was reached, the two solutions were mixed and the mixture was magnetically stirred until a homogeneous phase was obtained.

N-ADPA – *Nylon 6 and N-phenyl-1,4-phenylenediamine (ADPA)*: formic acid solutions of Nylon 6 (25 wt% with respect to formic acid) containing ADPA (67 wt% with respect to Nylon 6) were prepared.

N6 – *Nylon 6*: formic acid solutions of Nylon 6 (25 wt% with respect to formic acid) with no other additives were prepared.

Polymer fibers by electrospinning

Electrospinning was performed by loading the polymer solution in a 2.5 mL syringe with a 22 gauge needle (Hamilton Gastight model 1002 TLL), which was then mounted on a infusion pump (KDS Scientific, model series 200) that feeds the solution into the capillary nozzle at a constant flow rate of 0.05 mL h^{-1}. All the electrospinning runs were carried out at room temperature using a bottom-up vertical configuration. Voltage was applied to the needle by a High Voltage Power Supply (Spellman SL30P300). Fibers were collected randomly on glass and on silicon substrates; the best setup parameters are listed in Table 1.

Diffusion step

A diffusion bath containing an aqueous solution of *N*-phenyl-1,4-phenylenediamine (0.125 M) and HCl (0.175 M) was prepared and heated at 40 °C until complete dissolution. The N-FeH and N-sFeH electrospun fiber webs collected on a glass or silicon substrates were immersed in the solution. Samples were next rinsed in acetone and distilled water, and then dried with filter paper and stored under a hood for one night to ensure a gentle and complete drying.

Table 1 Electrospinning parameters of the preparation sets

Preparation	Voltage (kV)	Tip–collector distance (cm)	Flow rate (mL h^{-1})
N-FeA	15	20	0.05
N-FeH	15	20	0.05
N-sFeH	20	10	0.05
N-sADPA	17	10	0.05
N-ADPA	18	20	0.05
N6	18	20	0.05

Oxidative polymerization

Polymerization was performed by immersing the samples (i) after a diffusion step for N-sFeH set or (ii) as spun for N-sADPA set in an oxidation bath containing APS (0.125 M) and HCl (0.175 M) at 0 °C. The effect of other acids, such as oxalic acid and *p*-toluenesulfonic acid (*p*-TSA), keeping the molar concentration constant, was also tested.

This step was carried out in an ice bath[21,45] in order to slow down the reaction kinetics and gain better control over the polymerization rate. For the N-sFeH set, the oxidation time was set at 30 min. Conversely, different oxidation times were tested for N-sADPA as this procedure has not been investigated so far. The core/sheath fiber webs were then washed with distilled water, dried with filter paper and stored under a hood until the complete evaporation of the solvent.

Doping

Doping was carried out upon immersion of the samples in an acidic solution, followed by drying with filter paper to remove the excess acid. Different acids, including HCl, oxalic acid ($H_2C_2O_4$), sulfuric acid (H_2SO_4) and *p*-toluenesulfonic acid ($CH_3C_6H_4SO_3H$), were tested at different concentrations, namely 1 M, 0.5 M and 0.175 M.

Characterization

A high resolution scanning electron microscope (SEM), FEG LEO 1525 was used to collect electron micrographs of the electrospun fibers. No conductive coating was deposited onto the samples. The mean diameter and distribution from the SEM images were determined with the ImageJ software (Rasband, W.S., ImageJ, U. S. National Institutes of Health, Bethesda, Maryland, USA, http://rsb.info.nih.gov/ij/, 1997–2014). Contact angles (CA) were measured with an OCA system-DataPhysics according to the sessile method. Fourier transform infrared spectroscopy (FT-IR) was performed in transmission mode using a Nicolet NEXUS FTIR interferometer (DTGS detector) on free-standing electrospun membranes. The ADPA spectrum was collected from a drop cast film from acetone on the ZnSe substrate. The resolution was 0.1 cm^{-1} and 256 sample scans were acquired. The Omnic 7.1 software (Thermo Nicolet Instrumentation) was used to analyze the spectra. Ultraviolet-visible (UV-vis) absorption spectra were recorded on a Varian Cary 5000 spectrophotometer with the integrating sphere to measure the diffuse reflectance of the fiber mats.

Results and discussion

The electrospinning of conjugated polymers is generally rather demanding because of their limited solubility, relatively low molecular weight and rigid backbone. Among the possible methods reported in the literature to produce conjugated polymer fibers,[54–56] we referred to polymerization onto fiber templates, which allows the production of fibers with an insulating core and a conducting sheath. We have previously demonstrated that on exposing an electrospun polymer template containing an oxidizing salt to pyrrole vapours, a polymerization occurs at the fiber surface to afford Nylon 6/polypyrrole fibers.[53]

Herein we applied a similar procedure to produce polyaniline (PANI) fibers. Nylon 6 was chosen as a core polymer since it has been widely electrospun and the stability of polyamide to many solvents makes it suitable for a wide range of applications. The literature reports ammonium persulfate (APS) as the common oxidant employed in PANI synthesis.[29] However, APS cannot be directly dissolved in the Nylon 6 feed solution since formic acid reduces it to sulfate, disabling its ability to polymerize aniline. For this reason, iron(III) was used. Compared with APS, iron(III) chloride is characterized by a lower oxidation potential, which is not high enough to promote aniline polymerization. Interestingly, this problem can be overcome if, instead of aniline, *N*-phenyl-*p*-phenylenediamine ADPA is used as a starting monomer.[29]

Hexahydrate iron(III) chloride was preferred to the anhydrous one as the latter is highly hygroscopic. A good fiber morphology was obtained by using the same molar amount of anhydrous salt which has been tested in a previous work[53] (see ESI Fig. 1†). However, during the following polymerization steps, consisting in the monomer diffusion and oxidation in acidic medium, polyaniline growth suffered from poor control (see ESI Fig. 2†). We have tentatively ascribed this fact to the lack of a sufficient quantity of iron chloride onto the fiber surface to promote a uniform PANI polymerization. Acetone was added to the formic acid to promote segregation of the $FeCl_3{\cdot}6H_2O$ during the flight of the spun jet.[57] Surface segregation was expected to improve the polymerization efficiency, the quantity of salt available on the template surface being larger. The experimental flow chart of this strategy is shown in Scheme 1.

Acetone was chosen for the solvent induced segregation since it (i) easily dissolves hexahydrate iron(III) chloride, (ii) shows a boiling point (56 °C) lower than formic acid (100.8 °C), so it evaporates faster than the main solvent and (iii) it is a bad solvent for polyamides.

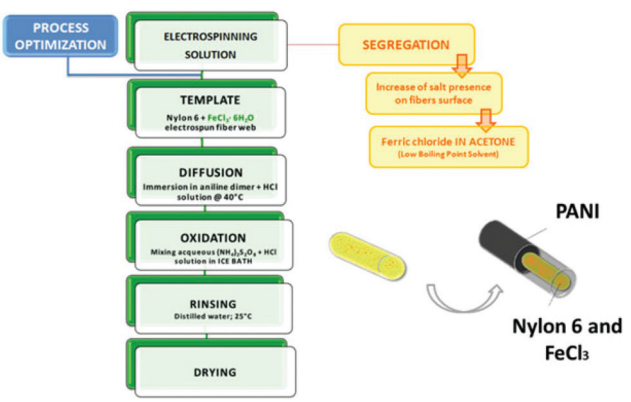

Scheme 1 Flow chart of the process to yield N-sFeH fibers. On the right: the sketch of the resulting core–sheath fiber mat.

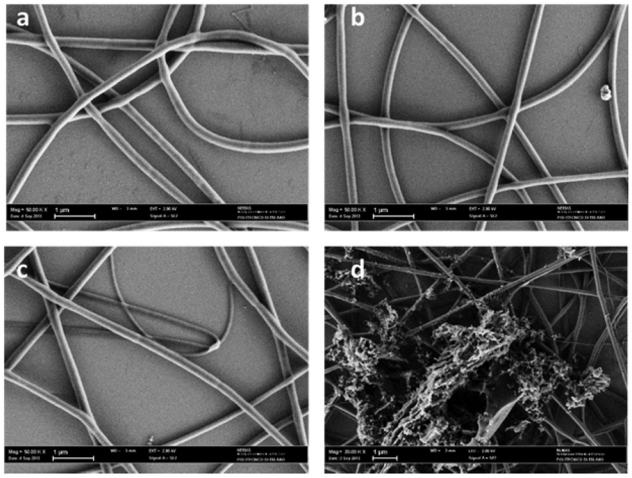

Fig. 1 Morphological characterization of N-sFeH (8.85 wt% $FeCl_3 \cdot 6H_2O$) electrospun nanofibers: (a) SEM image at 20 kV, a flow rate of 0.05 mL h^{-1} and a tip-collector distance of 10 cm. SEM images of N-sFeH electrospun nanofibers after a diffusion step of (b) 180′ and (c) 120′. (d) SEM images of N-sFeH electrospun nanofibers t_{DIFF} = 180′ + t_{OX} = 30′.

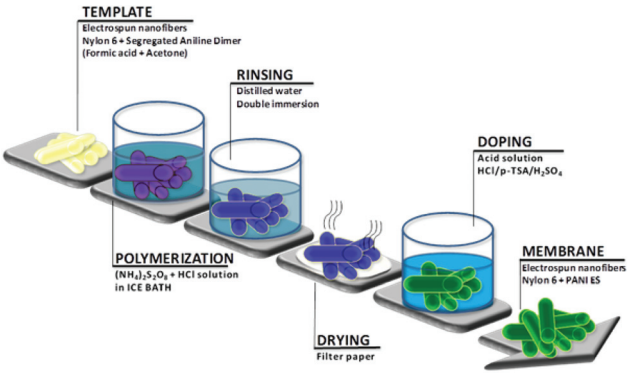

Scheme 2 Flow chart of the experimental process carried out on Nylon 6 and segregated ADPA blend.

The volume ratio between acetone and formic acid was optimized from 0 : 1 v/v to 3 : 7 v/v in order to dissolve the maximum quantity of $FeCl_3 \cdot 6H_2O$, while avoiding instability. The best condition was 2 : 7 v/v of acetone to formic acid ratio with 8.85 wt% of $FeCl_3 \cdot 6H_2O$ with respect to Nylon 6 (25 wt% with respect to formic acid).

The SEM analysis (see Fig. 1a) showed defect-free electrospun fibers with a mean diameter of 217 ± 40 nm.

The presence of segregated iron nanostructures cannot be highlighted by SEM due to the very thin nanofiber diameters. In the literature Nylon 6 is electrospun from hexafluoroisopropanol[58] to give fibers with larger diameters, thus allowing the investigation of the details of the fiber surface. However, $FeCl_3 \cdot 6H_2O$ is not soluble in hexafluoroisopropanol.

Immersion in an acidic aqueous solution of APDA for 120 and 180 minutes (t_{diff}) to promote diffusion of the aniline dimer onto the fiber surface and its possible polymerization did not affect fiber morphology and size. Statistical analysis of mean diameters for N-sFeH fibers at different diffusion times shows no significant changes of fiber diameter and morphology, as reported in Fig. 1b and c and ESI Fig. 9.†

This result led to the hypothesis that no polymerization occurred onto the fiber surface. Fibers were then immersed in an oxidation bath to further promote polymerization, but just new rough aggregates covered the fibrous mat (Fig. 1d oxidation time 30′ (t_{ox})). Despite fibers being expected to be likely coated by PANI, the presence of these large defective islands suggests a poor control over the polymerization and a low template induced-effect ruled by the Nylon/$FeCl_3$ mat.

Nylon 6 and segregated *N*-phenyl-1,4-phenylenediamine (ADPA) template nanofibers

As PANI did not uniformly coat fibers or, in the last case, no uniform control over the template polymerization was achieved, any procedure involving the addition of oxidant salts in the Nylon fiber template was not further considered. Alternatively, the feed solution was loaded with the aniline dimer instead of the oxidant and segregation was solvent-induced to maximize the dimer concentration at the surface. Afterwards, the fibrous template with the surface-segregated ADPA was polymerized upon immersion in the oxidation bath (Scheme 2). This procedure lowers the number of steps as the polymerization occurs in a single reaction bath containing both the oxidant salt and the acidic species without any diffusion step of the aniline monomer or dimer.

Template production

Different solutions of Nylon 6 (25 wt% with respect to formic acid) and ADPA in formic acid and acetone (ratio 2 : 7 (v/v) with respect to formic acid) were electrospun in order to determine the maximum loading concentration of ADPA (from 0 wt% to 73 wt% with respect to Nylon 6) to guarantee a stable electrospinning process. SEM images of the electrospun mats collected starting from different aniline dimer concentrations are shown in Fig. 2. Despite defect free fibers being obtained at every condition, electrospinning underwent instability when the aniline dimer concentration was increased to 73 wt%.

Interestingly, no segregated spot onto the fiber surface is evident, thus leading to the hypothesis that a uniform segregation at the fiber surface occurred. Electrospun nanofibers containing 67 wt% of ADPA (Fig. 2e) were considered for the following study.

To highlight the effect of ADPA segregation onto the fiber surface, analogous non-segregated N-ADPA mats were prepared, resulting in good fiber morphology also in this case (see ESI Fig. 3†).

Surface segregation of the aniline dimer during the fiber formation was monitored by contact angle (CA) measurements: a contact angle value of 122° was obtained for the pure Nylon 6 fiber mat, which is well consistent with that reported by Pant *et al.*[59] By addition of an aniline dimer into the feed solution, CA reduces till reaching a *plateau* at concentrations higher than 60 wt% (Fig. 3). Decreasing the contact angle while

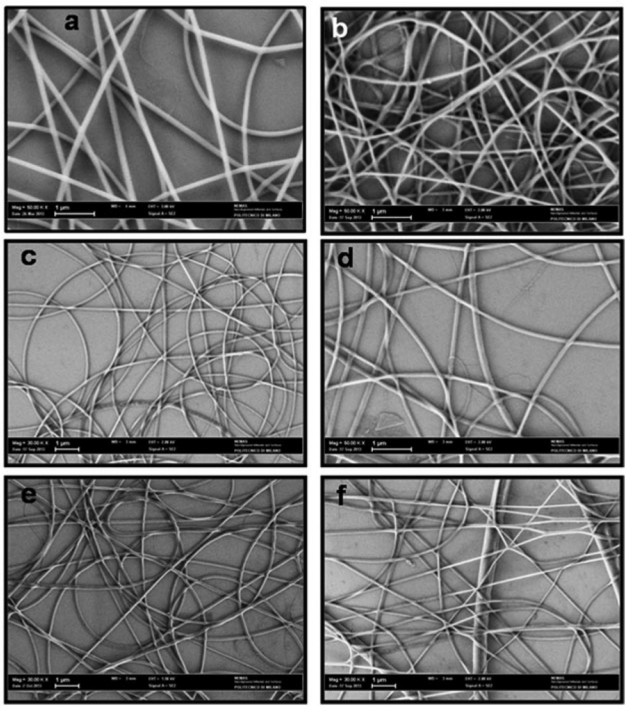

Fig. 2 SEM images of N-sADPA loaded with different ADPA concentrations: (a) 0%; (b) 48%; (c) 54%; (d) 60.5%; (e) 67%; (f) 73% wt% ADPA with respect to Nylon 6.

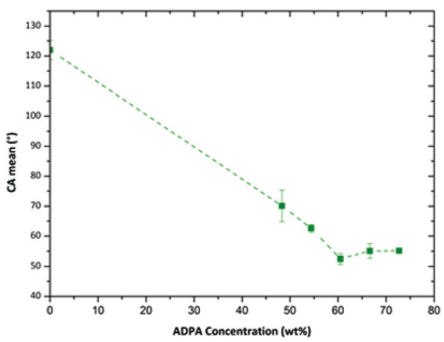

Fig. 3 Contact angle of Nylon 6 and N-sADPA electrospun nanofibers with different ADPA concentrations.

increasing surface segregation is related to the presence of amine groups in the *N*-phenyl-*p*-phenylenediamine.

UV-Vis spectra in diffuse reflectance were recorded on both fiber samples prepared with and without the presence of acetone in the feed solution. Fig. 4 reports the values $1-R$ (magnification of the visible region is reported in the ESI Fig. 4†).

The curve of the pure Nylon 6 mat (green line) shows the typical trend of a scattering material with no absorption in all the 250–2500 nm region.

In contrast, the absorption fingerprints at 290, 420 and 625 nm typical of ADPA are evident in N-sADPA and N-ADPA.[60]

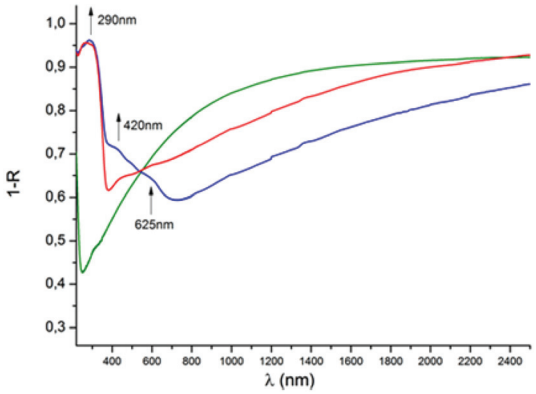

Fig. 4 UV-Vis diffuse reflectance spectra of Nylon 6 fiber mats (green line), N-sADPA (blue line) and N-ADPA (red line).

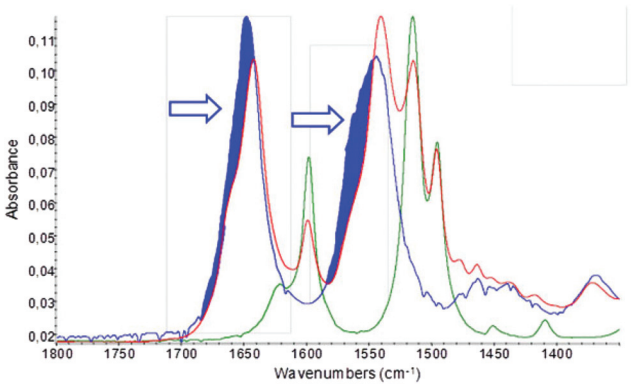

Fig. 5 FTIR spectra of electrospun N6 (blue line) and N-sADPA mats (red line), and ADPA film (green line). Narrowing of the amide I and amide II is highlighted in blue.

However, the relative intensity of these features differs between the segregated and non-segregated samples, the former being characterized by a higher absorption in the regions corresponding to the ADPA bands. This evidence demonstrates that the presence of acetone in the feed solution is effective in ADPA segregation at the fiber surface.

Relevant information on the interaction between polyamide and the aniline dimer was obtained from FTIR spectroscopy (Fig. 5). The detailed peak assignment of the two components is reported in Table 1 of the ESI.† It is worth noting that the bands associated with amide I and amide II vibrations (at 1650 and 1542 cm^{-1}, respectively) of the pure Nylon 6 mat are broad, being affected by all the possible conformations of the methylene segments. When Nylon 6 is loaded with ADPA, a significant sharpening of the amide I and II peaks is noted, which leads to the hypothesis that an interaction between the aniline dimer and nylon amide groups actually occurs that hampers some possible conformations in the polyamide chain. This hypothesis is further confirmed by the weakening of the N–H stretching of the aniline dimer (see ESI Fig. 5†).

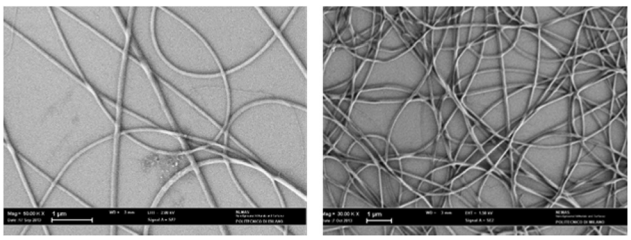

Fig. 6 N-sADPA (ADPA 67 wt% with respect to Nylon 6): on the left: SEM image after oxidative polymerization (t_{OX} = 150 s); on the right: after doping in HCl (0.175 M).

Oxidative polymerization

Upon immersion of N-sADPA (67 wt% ADPA/Nylon 6) in the oxidation bath, polymerization occurred at the fiber surface. Oxidation bath temperature was set to 0 °C since at room temperature the polymerization kinetics is too fast.

Immersion in the oxidative bath was varied from 30 s, 150 s, 300 s, 450 s to 600 s to determine the best time scale for polymerization to be completed while avoiding an over-oxidation of the PANI.[29]

Polymerization does not affect either the fibrous morphology or fiber size distribution (Fig. 6 and ESI Fig. 10†). By statistical analysis of the electrospun mats it turns out that the mean fiber diameter was equal to 160 ± 30 nm before polymerization and 150 ± 30 nm after oxidative polymerization. Therefore, the final PANI mat has a similar diameter distribution to the Nylon 6 template. Acting on the solution parameters, such as polymer concentration, and processing conditions as voltage and flow rate, it is possible to control the fiber diameter of the final mat.

During polymerization by immersion in APS (0.125 M) and HCl (0.175 M) bath the ivory fibrous membrane turned dark grey immediately after the immersion, then pale blue. After rinsing in water and drying, the final color of the mat was bluish, typical of the emeraldine base (Fig. 7).

The effects of other acids, such as oxalic acid or *p*-toluenesulfonic acid (*p*-TSA), were tested (0.175 M). The former showed poor solubility under the polymerization conditions, whereas fibers were successfully polymerized with *p*-TSA. Despite fibrous morphology being retained after oxidation, SEM images showed the presence of some shining spots, probably associated with residual *p*-TSA (see ESI Fig. 6†).

The formation of PANI onto the fiber surface upon immersion of the mat in the oxidation bath containing APS (0.125 M)

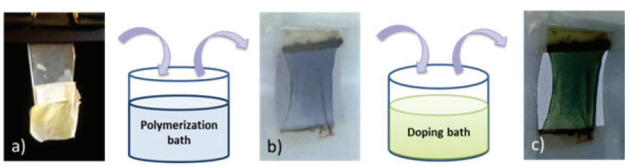

Fig. 7 Colour turning of the N-sADPA electrospun nanofibrous membrane after oxidative polymerization and doping steps: (a) free-standing fibrous membrane as spun; (b) after oxidative polymerization step: t_{OX} = 150 s in APS (0.125 M) and HCl (0.175 M); (c) after the following doping step: t_{DOP} = 30 s in HCl (0.175 M).

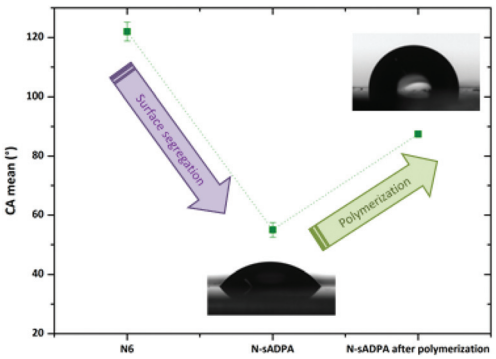

Fig. 8 Contact angle (CA) measurements of the N6 nanofiber mat, as-spun N-sADPA mat, N-sADPA mat after oxidation in APS (0.125 M) for 150 s. Each value arises from the average of at least ten measurements on different points of the same sample.

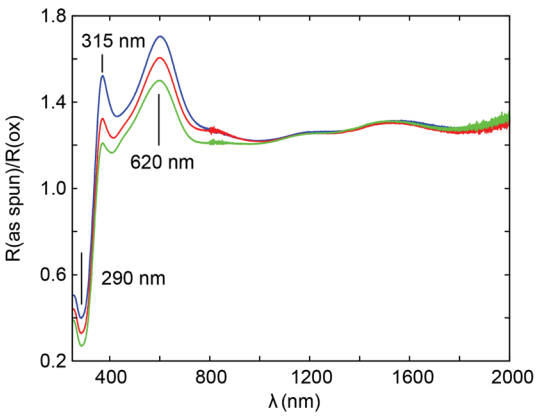

Fig. 9 UV-Vis reflectance spectra of N-sADPA (67 wt% ADPA *vs.* Nylon 6) electrospun nanofibers t_{OX} = 20 s (blue); t_{OX} = 50 s (red); t_{OX} = 120 s (green). *R* (as spun)/*R* (ox) spectra.

and HCl (0.175 M) was monitored by contact angle measurements with UV-Vis and infrared spectroscopy.

The CA value of the electrospun mat increases after polymerization (see Fig. 8), as the primary amine groups of ADPA react during the oxidation step.

UV-Vis spectra collected in diffuse reflectance mode of samples after 20, 50 and 120 seconds of immersion in the polymerization bath were recorded. Relative spectra obtained as the ratio *R*(as spun)/*R*(ox) to avoid the scattering issue and highlight the differences are reported in Fig. 9 (as recorded spectra is reported in ESI Fig. 7†).

The growth of absorption bands at 315 nm and at 620 nm is consistent with the electronic transitions in the emeraldine base,[61,62] as sketched in Fig. 10, while the decrease in absorption at 290 nm indicates that the ADPA was exhausted during polymerization.[63,64]

Although UV-Vis reflectance spectroscopy clearly demonstrates the occurrence of polymerization, the kinetics of the process could not be quantitatively determined as spectra suffer from the scattering due to the fibrous morphology, and a common baseline could not be set.

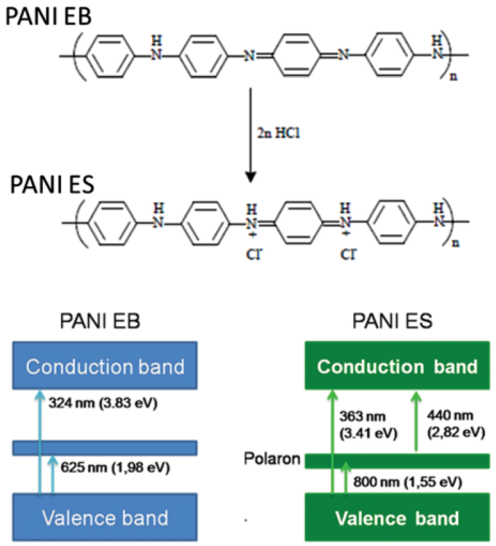

Fig. 10 Energy diagrams and molecular structure of PANI before doping (emeraldine base form EB) and after doping with HCl (emeraldine salt ES) (values of level transitions adapted from the literature[66]).

Conversely, it is possible to monitor the reaction proceeding by IR spectroscopy, following some vibrational modes which are strongly modified during the PANI formation (Fig. 11).

A gradual disappearance of the peaks near 1600 cm^{-1} occurs, which are fingerprints of the aniline dimer. These features are associated with the aromatic ring stretching and the N–H bending of the primary amine ($-NH_2$), which is the functional group involved in the polymerization reaction. This band totally disappears after 150 s of polymerization, so this time was adopted as the optimal to complete the polymerization.

For a prolonged oxidation time (t_{OX} = 150 s), a band at 1147 cm^{-1} is observed, which has been assigned, according to ref. 67, to the vibrations of the positively charged polymer units Q═NH^+–B or B–$NH^{+\bullet}$–B, where Q indicates a quinoid

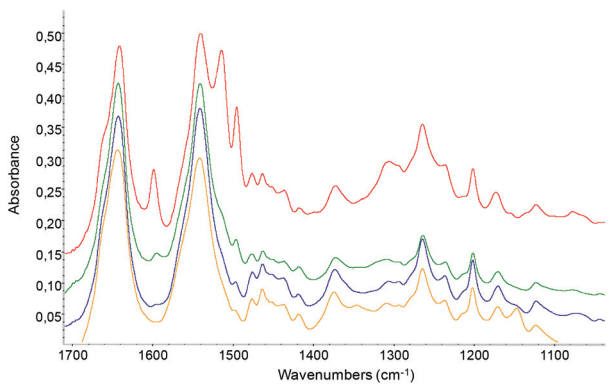

Fig. 11 FTIR spectra of N-sADPA (67 wt% ADPA *vs.* Nylon 6) in wavenumbers range 1700–500 cm^{-1} at different oxidation times: before oxidation step (red); t_{OX} = 10 s (green); t_{OX} = 30 s (blue); t_{OX} = 150 s (orange).

structure while B, the benzenoid one. It means that a slight protonation may accompany oxidation, which is reasonable since polymerization occurs in an acidic environment. Although this assignment could be an object of criticism since many vibrations lie in this frequency range, this hypothesis has also been confirmed by the spectra collected after a base treatment (see ESI Fig. 11† on the right), which was carried out upon immersion of the sample in an aqueous solution of KOH (0.175 M). The band at 1147 cm^{-1} completely disappears, thus indicating that alkaline treatment has effectively removed the partial doping.

Doping step

In order to convert polyaniline from the blue emeraldine base form to the conductive green emeraldine salt, a doping process was carried out in an acidic environment. 1 M and 0.5 M HCl was too aggressive and a damage of the fabric was observed. Immersion into the 0.175 M HCl doping bath, which is the same concentration used in the polymerization, did not affect the homogeneity and uniformity of the mat (see Fig. 6 on the right). To avoid possible damaging of the fibers, the excess of acid was removed by drying the fibrous mat onto an absorbing paper. Doping time was set at 30 s.

The statistical analysis on the diameters evidenced that the distribution frequency, with average diameter of 140 ± 20 nm, did not change by doping (see ESI Fig. 10†). Doping was also performed with oxalic acid, *p*-TSA and sulfuric acid and similar results have been obtained in all cases.

It is known that doping leads to the formation of charged species (*e.g.* polarons and bipolarons) which are evidenced by the appearance of a broad electronic band at longer wavelengths in the UV-vis spectra. As regards PANI, the position of the polaronic absorption bands shifts to a longer wavelength while increasing the size of the dopant. Specifically, PANI doped with a smaller dopant shows a polaronic band located at 800–900 nm, whereas a band above 1000 nm characterizes PANI doped with a larger dopant.[29,65]

In the UV-Vis spectra (Fig. 12), the band at 620 nm characteristic of PANI emeraldine base disappears with HCl doping, while two bands at *ca.* 800 nm and 400 nm were found, the latter being ascribed to a convolution of the two bands at *ca.* 360 nm and at 440 nm which are related to the π–π* and polaron–π* transitions, respectively[68] (as recorded spectra are reported in ESI Fig. 8†). The band at lower energy (*e.g.* 800 nm) is related to π–polaron transition. For the sake of clarity, the energy diagram for PANI-ES is reported in Fig. 10. Interestingly, the doped material evolved with time and, in the spectrum collected one hour later, some bands slightly arise in the region of 1000–1500 nm, whose appearance may be ascribed to the relaxation along the chain structure of polarons and bipolarons.

The modifications of the IR spectra induced by doping involve different vibrational modes; indeed, it is expected that a large portion of the spectrum changes upon doping as the size of the polaron and bipolaron is large, thus involving several chemical units; within this frequency range, many

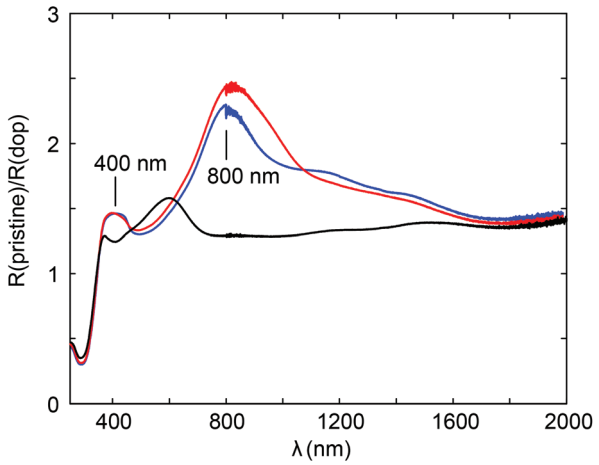

Fig. 12 UV-Vis reflectance spectra N-sADPA (67 wt% ADPA *vs*. Nylon 6) electrospun nanofibers: t_{OX} = 150 s (black); t_{DOP} = 60 s (red); t_{DOP} = 60 s after 1 h (blue). *R* (pristine)/*R* (doped) spectra.

weak, medium, and sometimes very strong bands may be observed. A school of thought[69] claims that the doping induced infrared spectrum is only the result of a "spreading" of the electronic intensity on the infrared spectra. The phenomenon is called "Fano resonance" and is still under study for simple systems.

Samples were analyzed immediately after the doping step, once the membranes were dried. The collected spectra of the protonated samples are reported in Fig. 13.

Looking at the range of the spectrum from *ca.* 1400 to *ca.* 900 cm^{-1} as arising from the vibrations of polarons or bipolarons, HCl and H_2SO_4 were revealed to be weak doping agents because band intensities related to the protonated emeraldine salt do not significantly increase. Protonation still remains not efficient even if the dopant concentration increases.

Conversely, *p*-TSA turned out to be a more efficient doping agent than HCl or H_2SO_4 as the IR spectrum shows a strong doping-induced increase in intensity.

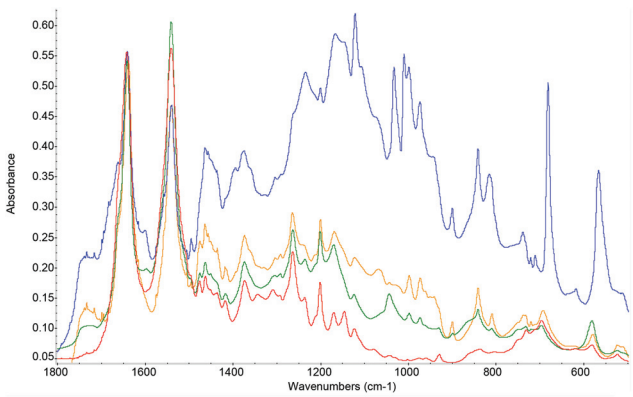

Fig. 13 FTIR spectra in wavenumbers range 1800–500 cm^{-1} before doping (red) and after doping: t_{DOP} = 30 s in H_2SO_4 0.175 M (green); t_{DOP} = 30 s in HCl 0.175 M (orange); t_{DOP} = 30 s in *p*-TSA 0.175 M (blue).

Incidentally, for some dopants own normal modes may be recognized with a few characteristic bands which do originate from motions localized right in the counterion. These particular features can be well observed in the case of *p*-TSA: the hydrogen sulfonate counterion of tosylate may be evidenced by the band at 1040 cm^{-1} that is attributed to the symmetric SO_3 stretching. New bands appear at 900 cm^{-1} and 560 cm^{-1} by doping and both are due to the SO^{3-} group of *p*-TSA.[29]

Conclusions

Homogeneous and defect-free emeraldine salt PANI nanofibrous membranes consisting of a Nylon 6 core and a polyaniline (PANI) sheath were demonstrated by means of electrospinning combined with template polymerization. Although the general procedure could consist of the introduction of an oxidant salt that promotes the polymerization in the feed solution to be electrospun, this strategy turned out to be not successful even in the case of the segregation of $FeCl_3{\cdot}6H_2O$ onto the fiber surface. Nevertheless, segregation was exploited in the new two-step process herein proposed where *N*-phenyl-1,4-phenylenediamine (ADPA) is loaded into the Nylon 6 feed solution and then polymerized upon immersion of the composite fibers into a solution containing an oxidant and an acidic species. The control over the process resulted to be excellent, providing homogeneous fibers which maintained the same morphology during the polymerization step. Formation of a PANI sheath onto the fiber surface was demonstrated by monitoring the polymerization by UV-Vis and FTIR spectroscopy. The composite Nylon 6/PANI nanofibrous membranes were doped to give the emeraldine salt. Among the different acids, the most effective doping has been obtained with *p*-TSA.

The method herein proposed provides an easy, simple, rapid route to the production of remarkable free-standing emeraldine salt PANI membranes which, combining the high surface to volume ratio of the elctrospun mats with the versatility of polyaniline coating, leads to potential developments in biological applications, chemical sensors and filtration of hazardous elements.

Acknowledgements

Fondazione Cariplo is acknowledged for the financial support through the InDiXi project grant no. 2011-0368.

Notes and references

1 Z.-M. Huang, Y.-Z. Zhang, M. Kotaki and S. Ramakrishna, *Compos. Sci. Technol.*, 2003, **63**, 2223–2253.

2 C. P. Grey, S. T. Newton, G. L. Bowlin, T. W. Haas and D. G. Simpson, *Biomaterials*, 2013, **34**, 4993–5006.

3 Y. Sharma, A. Tiwari, S. Hattori, D. Terada, A. K. Sharma, M. Ramalingam and H. Kobayashi, *Int. J. Biol. Macromol.*, 2012, **51**, 627–631.
4 Y. Liao, X.-G. Li, E. M. V. Hoek and R. B. Kaner, *J. Mater. Chem. A*, 2013, **1**, 15390.
5 X.-H. Qin and S.-Y. Wang, *J. Appl. Polym. Sci.*, 2006, **102**, 1285–1290.
6 P. Gibson, H. Schreuder-Gibson and D. Rivin, *Colloids Surf., A.*, 2001, **187–188**, 469–481.
7 H. Fong, W. Liu, C. Wang and R. A. Vaia, *Polymer*, 2002, **43**, 775–780.
8 L. Liu, Z.-M. Huang, C. L. He and X. J. Han, *Mater. Sci. Eng., A*, 2006, **435–436**, 309–317.
9 M. Stasiak, A. Studer, A. Greiner and J. H. Wendorff, *Chemistry*, 2007, **13**, 6150–6156.
10 T. J. Sill and H. A. von Recum, *Biomaterials*, 2008, **29**, 1989–2006.
11 J. Pelipenko, P. Kocbek, B. Govedarica, R. Rošic, S. Baumgartner and J. Kristl, *Eur. J. Pharm. Biopharm.*, 2013, **84**, 401–411.
12 K. S. Rho, L. Jeong, G. Lee, B.-M. Seo, Y. J. Park, S.-D. Hong, S. Roh, J. J. Cho, W. H. Park and B.-M. Min, *Biomaterials*, 2006, **27**, 1452–1461.
13 Y. Zhou, H. Yang, X. Liu, J. Mao, S. Gu and W. Xu, *Int. J. Biol. Macromol.*, 2013, **53**, 88–92.
14 H. Yoshimoto, Y. M. Shin, H. Terai and J. P. Vacanti, *Biomaterials*, 2003, **24**, 2077–2082.
15 S. Ramakrishna, K. Fujihara, W. E. Teo, T. C. Lim and Z. Ma, *An Introduction to Electrospinning and Nanofibers*, World Scientific Publishing, 2005.
16 C. J. Luo, S. D. Stoyanov, E. Stride, E. Pelan and M. Edirisinghe, *Chem. Soc. Rev.*, 2012, **41**, 4708–4735.
17 A. Greiner and J. H. Wendorff, *Angew. Chem. Int. Ed.*, 2007, **46**, 5670–5703.
18 W. E. Teo and S. Ramakrishna, *Nanotechnology*, 2006, **17**, R89–R106.
19 J. T. McCann, D. Li and Y. Xia, *J. Mater. Chem.*, 2005, **15**, 735.
20 X. Wang, C. Drew, S.-H. Lee, K. J. Senecal, J. Kumar and L. A. Samuelson, *Nano Lett.*, 2002, **2**, 1273–1275.
21 Q. Wang, X. Dong, Z. Pang, Y. Du, X. Xia, Q. Wei and F. Huang, *Sensors*, 2012, **12**, 17046–17057.
22 H. Bagheri and A. Aghakhani, *Anal. Chim. Acta*, 2012, **713**, 63–69.
23 H. Dong, U. Megalamane and W. Jones, in *Abstract of Papers of the American Chemical Society*, 2003, vol. 226, p. 1155.
24 H. Bai, L. Zhao, C. Lu, C. Li and G. Shi, *Polymer*, 2009, **50**, 3292–3301.
25 A. A. Syed and M. K. Dinesan, *Synth. Met.*, 1990, **36**, 209–215.
26 Z. Chen, C. Dellapina, E. Falletta, M. Lofaro, M. Pasta, M. Rossi and N. Santo, *J. Catal.*, 2008, **259**, 1–4.
27 H. Wang, L. Ji, D. Li and J.-Y. Wang, *J. Phys. Chem. B*, 2008, **112**, 2671–2677.
28 Y. Xia, J. M. Wiesinger, A. G. Macdiarmid and A. J. Epstein, *Chem. Mater.*, 1995, **7**, 443–445.
29 R. W. Gumbs, in *Handbook of organic conductive molecules and polymers – vol 2*, ed. H. S. Nalwa, John Wiley, 1997, pp. 505–572.
30 Y. Niu, *Polym. Eng. Sci.*, 2008, **48**, 355–359.
31 M. Jaymand, *Prog. Polym. Sci.*, 2013, **38**, 1287–1306.
32 A. G. Macdiarmid and A. J. Epstein, *Faraday Discuss. Chem. Soc.*, 1989, **88**, 317–332.
33 Q. Lin, Y. Li and M. Yang, *Sens. Actuators, B*, 2012, **161**, 967–972.
34 I. Sapurina and J. Stejskal, *Polym Int.*, 2008, **57**, 1295–1325.
35 L. Zhang, H. Peng, P. A. Kilmartin, C. Soeller, R. Tilley and J. Travas-Sejdic, *Macromol. Rapid Commun.*, 2008, **29**, 598–603.
36 N. V. Blinova, J. Stejskal, M. Trchová, I. Sapurina and G. Ćirić-Marjanović, *Polymer*, 2009, **50**, 50–56.
37 Y. Zhang, Q. Li, L. Sun, R. Tang and J. Zhai, *J. Hazard. Mater.*, 2010, **175**, 404–409.
38 R. Li, L. Liu and F. Yang, *Chem. Eng. J.*, 2013, **229**, 460–468.
39 S. Bozkir, M. Sankir, L. Semiz, N. D. Sankir and A. Usanmaz, *Polym. Eng. Sci.*, 2012, **52**, 1613–1620.
40 M. Sankır, S. Bozkır and B. Aran, *Desalination*, 2010, **251**, 131–136.
41 A. Bianco, C. Bertarelli, S. Frisk, J. Rabolt, M. Gallazzi and G. Zerbi, *Synth. Met.*, 2007, **157**, 276–281.
42 I. D. Norris, M. M. Shaker, F. K. Ko and A. G. MacDiarmid, *Synth. Met.*, 2000, **114**, 109–114.
43 M. P. Prabhakaran, L. Ghasemi-Mobarakeh, G. Jin and S. Ramakrishna, *J. Biosci. Bioeng.*, 2011, **112**, 501–507.
44 E. Zampetti, A. Muzyczuk, A. Macagnano, S. Pantalei, S. Scalese, C. Spinella and A. Bearzotti, *J. Nanopart. Res.*, 2011, **13**, 6193–6200.
45 M. J. D. León, *Proc. Natl. Conf. Undergrad. Res.*, 2001, **1**, 1–5.
46 Y. Zhang and G. C. Rutledge, *Macromolecules*, 2012, **45**, 4238–4246.
47 H. Dong, V. Nyame, A. G. MacDiarmid and W. E. Jones, *J. Polym. Sci., Part B: Polym. Phys.*, 2004, **42**, 3934–3942.
48 M. Wei, J. Lee, B. Kang and J. Mead, *Macromol. Rapid Commun.*, 2005, **26**, 1127–1132.
49 M. Wei, B. Kang, C. Sung and J. Mead, *Macromol. Mater. Eng.*, 2006, **291**, 1307–1314.
50 K. H. Hong, K. W. Oh and T. J. Kang, *J. Appl. Polym. Sci.*, 2005, **96**, 983–991.
51 D. Chen, Y. Miao and T. Liu, *ACS Appl. Mater. Interfaces*, 2013, **5**, 1206–1212.
52 F. Granato, M. Scampicchio, A. Bianco, S. Mannino, C. Bertarelli and G. Zerbi, *Electroanalysis*, 2008, **20**, 1374–1377.
53 F. Granato, A. Bianco, C. Bertarelli and G. Zerbi, *Macromol. Rapid Commun.*, 2009, **30**, 453–458.
54 H. Liu, J. Kameoka, D. A. Czaplewski and H. G. Craighead, *Nano Lett.*, 2004, **4**, 671–675.
55 A. Laforgue and L. Robitaille, *Synth. Met.*, 2008, **158**, 577–584.

56 E. V. Canesi, A. Luzio, B. Saglio, A. Bianco, M. Caironi and C. Bertarelli, *ACS Macro Lett.*, 2012, **1**, 366–369.

57 S. Nair, E. Hsiao and S. H. Kim, *J. Mater. Chem.*, 2008, **18**, 5155.

58 A. Cho, D. M. Shin, H. W. Jung, J. C. Hyun, J. S. Lee, D. Cho and Y. L. Joo, *J. Appl. Polym. Sci.*, 2011, **120**, 752–758.

59 H. R. Pant, H. J. Kim, L. R. Bhatt, M. K. Joshi, E. K. Kim, J. I. Kim, A. Abdal-hay, K. S. Hui and C. S. Kim, *Appl. Surf. Sci.*, 2013, 4–10.

60 A. P. Monkman, D. Bloor, G. C. Stevens, J. C. H. Stevens and P. Wilson, *Synth. Met.*, 1989, **29**, 277–284.

61 J. Libert, J. Cornil, D. dos Santos and J. Brédas, *Phys. Rev. B: Condens. Matter*, 1997, **56**, 8638–8650.

62 R. McCall, J. Ginder, J. Leng, H. Ye, S. Manohar, J. Masters, G. Asturias, A. MacDiarmid and A. Epstein, *Phys. Rev. B: Condens. Matter*, 1990, **41**, 5202–5213.

63 N. Gospodinova and L. Terlemezyan, *Prog. Polym. Sci.*, 1998, **23**, 1443–1484.

64 J. Libert, J. Cornil, D. dos Santos and J. Brédas, *Phys. Rev. B: Condens. Matter*, 1997, **56**, 8638–8650.

65 A. G. MacDiarmid and A. J. Epstein, *Synth. Met.*, 1994, **65**, 103–116.

66 *Nanostructured Conductive Polymers*, ed. A. Eftekhari, Department of Chemistry, Ohio Institute of Technology, Cleveland, Ohio, USA, 2010.

67 G. Cirić-Marjanović, M. Trchová, E. N. Konyushenko, P. Holler and J. Stejskal, *J. Phys. Chem. B*, 2008, **112**, 6976–6987.

68 W. S. Huang and A. G. MacDiarmid, *Polymer*, 1993, **34**, 1833–1845.

69 B. Horovitz, R. Österbacka and Z. V. Vardeny, *Synth. Met.*, 2004, **141**, 179–183.